Journal of Photochemistry & Photobiology, B: Biology 260 (2024) 113043

Contents lists available at ScienceDirect

Journal of Photochemistry & Photobiology, B: Biology

journal homepage: www.elsevier.com/locate/jphotobiol

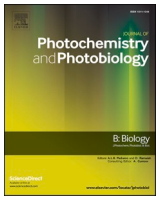

Metataxonomy and pigments analyses unravel microbial diversity and the relevance of retinal-based photoheterotrophy at different salinities in the Odiel Salterns (SW, Spain)

Patricia Gómez-Villegas [a], Miguel Pérez-Rodríguez [b], Jesús M. Porres [c], José C. Prados [d], Consolación Melguizo [d], Javier Vigara [a], Ignacio Moreno-Garrido [e], Rosa León [a,*]

[a] Laboratory of Biochemistry, Center for Natural Resources, Health and Environment (RENSMA), University of Huelva, 21071 Huelva, Spain
[b] Department of Cell Biology, Physiology and Immunology, University of Córdoba, Campus de Excelencia Internacional Agroalimentario CeiA3, Córdoba, Spain
[c] Department of Physiology, Institute of Nutrition and Food Technology (INyTA), Biomedical Research Center (CIBM), Universidad de Granada, 18100 Granada, Spain
[d] Department of Anatomy and Embryology, Faculty of Medicine, Institute of Biopathology and Regenerative Medicine (IBIMER), Biomedical Research Center (CIBM), Universidad de Granada, 18100 Granada, Spain
[e] Institute of Marine Sciences of Andalusia (CSIC), Campus Univ. Río San Pedro, Puerto Real, 11519 Cádiz, Spain

ARTICLE INFO

Keywords:
Brines
Halophiles
Pigments
Photosynthesis
Photoheterotrophy
Retinal
rRNA metataxonomy

ABSTRACT

Salinity has a strong influence on microorganisms distribution patterns and consequently on the relevance of photoheterotrophic metabolism, which since the discovery of proteorhodopsins is considered the main contributor to solar energy capture on the surface of the oceans. Solar salterns constitute an exceptional system for the simultaneous study of several salt concentrations, ranging from seawater, the most abundant environment on Earth, to saturated brine, one of the most extreme, which has been scarcely studied. In this study, pigment composition across the salinity gradient has been analyzed by spectrophotometry and RP-HPLC, and the influence of salinity on microbial diversity of the three domains of life has been evaluated by a metataxonomic study targeting hypervariable regions of 16S and 18S rRNA genes. Furthermore, based on the chlorophyll *a* and retinal content, we have estimated the relative abundance of rhodopsins and photosynthetic reaction centers, concluding that there is a strong correlation between the retinal/chlorophyll *a* ratio and salinity. Retinal-based photoheterotrophy is particularly important for prokaryotic survival in hypersaline environments, surpassing the sunlight energy captured by photosynthesis, and being more relevant as salinity increases. This fact has implications for understanding the survival of microorganisms in extreme conditions and the energy dynamics in solar salter ponds.

1. Introduction

Photosynthesis is the main biological process by which sunlight is captured and converted into chemical energy on Earth. However, in the photic zone of oceanic and continental waters, the importance of chlorophylls-based light energy transduction systems has to compete with retinylidene rhodopsins, which are the main contributors to photoherotrophic metabolism [1]. The first light-driven ion-pumping rhodopsins were discovered in the 70s in haloarchaea [2]. Nevertheless, photosynthesis continued to be considered the main mechanism involved in capturing sunlight in marine environments, and phytoplankton (cyanobacteria, photosynthesizing bacteria, and microalgae) the main responsible for light energy transduction in the sea, until the discovery that proteorhodopsins are widely distributed in many marine microorganisms [3–5]. We now know that retinylidene rhodopsins are present in many different taxonomic groups, including bacteria, archaea, and unicellular eukaryotes, and that they are involved in a variety of light-driven functions, such as protons, sodium, and chloride pumping, light sensing, gene regulation, phototaxy or other energy-demanding processes [6,7].

The systematic analysis of metagenomic data revealed that the genes encoding proton-pumping rhodopsins are present in more than half of all the heterotrophic bacteria and archaea inhabiting the ocean surface [1,8–10], where they capture sunlight to pump protons extracellularly and create a proton gradient that drives the production of ATP, allowing these microorganisms to get some extra energy when nutrients are

* Corresponding author.
E-mail address: rleon@uhu.es (R. León).

https://doi.org/10.1016/j.jphotobiol.2024.113043
Received 21 July 2024; Received in revised form 10 October 2024; Accepted 14 October 2024
Available online 17 October 2024

scarce [6]. Considering that retinal is equimolarly bonded to rhodopsins and that there are around 300 molecules of chlorophyll *a* per reaction center in oxygenic photosynthetic organisms, Gómez-Consarnau and cowokers followed a non-genomic approach for the chemical quantification of the different light-energy transducing systems along the Mediterranean Sea. They confirmed that the contribution of retinal-based energy harvested by aquatic heterotrophic organisms can be even superior to that of chlorophyll-based photosynthesis on the ocean surface, and demonstrated that rhodopsins-based capture of light, far from being a rarity as previously thought, constitutes the main energy input in the oceans [11].

Another important milestone in understanding rhodopsin function was the discovery that some ketocarotenoids [5] and hydroxylated carotenoids [12] can act as auxiliary antenna chromophores, transferring light energy to retinal. It has been estimated that about half of the known rhodopsins could interact with a carotenoid secondary antenna [12]. The distribution of pigments in seawater has been thoroughly studied and traditionally used as a taxonomic indicator for phytoplankton [13]. Pigments produced by halophilic bacteria and haloarchaea have also received attention [14], however, their comparative distribution in response to salinity at high salt concentrations has been scarcely explored. Similarly, most studies about the levels of rhodopsins or retinal have focused on open oceanic or brackish waters [8], but curiously, despite the fact that the first proton-pumps rhodopsins were found in hypersaline media, rhodopsins abundance in these environments has not been studied so far.

Salinity has a strong influence on the distribution patterns of microorganisms, and consequently on the relative relevance of photoautotrophic and photoheterotrophic light capture. However, only a limited number of studies have documented the complete microbial diversity, including the three domains of life, along the salinity gradient [15–17]. Most existing studies are focused on the prokaryotic microbial community at very high salinity [18–20], while the population of eukaryotic microorganisms in hypersaline waters have been often underestimated [21–24].

Our studies have been focused on the Odiel Salterns, located on the Atlantic coast in the Southwest of Spain. We have previously demonstrated that crystallization ponds of the Odiel Marshlands harbor a variety of halophilic microorganisms that have developed original mechanisms to cope with high salinity, which usually involve enzymes adapted to work at high salt concentrations [25] and new metabolites with potential industrial and health applied bioactivities [26]. However, Atlantic solar salterns, remain sparsely described [27] and the characterization of the microbial community of Odiel Salterns at the growing salinity gradient is not completed. The microbial profile and the relevance of photoherotrophic light capture by retinylidene photoproteins at environments of different salinities have implications for understanding the survival of microorganisms at extreme conditions. In addition, understanding the energy dynamics in solar salter ponds can help to optimize their performance.

In the present work, we have addressed some of the topics understudied in hypersaline environments, analyzing the pigment composition at different salinities and studying, by a 16S/18S metabarcoding analysis, the influence of salinity on the prokaryotic and eukaryotic microbial population. Moreover, we performed a systematic determination of the concentration of chlorophyll *a* and the apocarotenoid retinal at different salinities, and following the approach proposed by Gómez-Consarnau and coworkers [11], we estimated the relative abundance of rhodopsins and photosynthetic reaction centers to uncover the relative significance of the different light energy photoconversion mechanisms at different salinities, establishing a correlation between the retinal/ chlorophyll *a* ratio and salinity in Odiel Saltworks.

2. Materials and Methods

2.1. Sampling and Physico-Chemical Analyses of Water

Water samples were collected at the beginning of summer (July) from four different ponds with increasing salinities of Odiel Salterns, located in the estuary of Odiel and Tinto Rivers in the Odiel Marshes Nature Reserve near the city of Huelva, SW Spain (37.255787, −6.971191). Samples were collected in triplicate from the surface layer of the water in sterile 5 L plastic tanks and transported to the lab for processing. The physicochemical parameters conductivity (EC, μS cm^{-1}), pH, and temperature (T, °C), were determined in situ by a portable multimeter (Hanna HI98195). Density (g mL^{-1}) and ionic composition of the brine were measured following the standard methods as previously reported [28].

2.2. Flow Cytometry

Non-fixed samples were filtered by a 20 μm Nylon mesh before being analyzed in an Accuri C6 (Becton Dickinson) flow cytometer. FL2 (585 nm / 40 nm window wavelength) and FL3 (670 nm / Long Pass Filter) signals were plotted versus Side Scatter signal, in order to detect and count particles showing phycoerythrin (orange) and chlorophyll (red) fluorescence, respectively. 100 μL were analyzed per sample in triplicate to calculate cellular density. Controls (Milli-Q ultrapure water, not plotted in the text) were also analyzed to ensure the absence of instrumental background noise.

2.3. Pigment and Retinal Determination

Pigments and retinal were extracted from 12 samples from four different sampling points: Seawater inlet (SI), Evaporation pond 1 (EP1), Evaporation pond 2 (EP2), and Crystallization pond (CP), and analyzed by HPLC. Microbial biomass was collected by filtration using 0.45 μm Whatman® glass microfiber filters (GF/F) until filter saturation, with a final filtered volume of 2 L for sample SI, 200 mL for sample EP1, 700 mL for EP2, and 600 mL for sample CP, in triplicate for every pigment and retinal extractions. Each filter was treated with 5 mL of cold acetone (−20 °C) overnight to extract the pigments. Subsequently, the samples were centrifuged to separate acetone fractions from cellular debris and the obtained supernatant was used for the analysis of the pigments. For an efficient extraction of retinal as retinal oxime, hydroxylamine was added to the extraction solution. Since acetone has been found to react with hydroxylamine, in this study we used a solution of chloroform/methanol instead [29]. Each filter was treated with 5 mL chloroform/methanol (2:1, *v*/v) and 50 μL of 1 M hydroxylamine-HCl in 1 M Tris-HCl (pH 8). The suspension was sonicated for 5 min, incubated in light (150 $\mu mol/m^{-2}/s^{-1}$) for one hour, and centrifuged. The supernatant was collected, evaporated, dissolved in 500 μL methanol, and subjected to HPLC analysis.

The absorbance profile of each sample was recorded in an Ultrospec 3100 pro UV/visible spectrophotometer and the chromatographic analysis of pigments was performed in a Merck Hitachi HPLC equipped with a DAD detector, using an RP-18 column and a flow rate of 1 mL min^{-1}. Solvents were (A) a mixture of acetonitrile/water (9:1 *v*/v) and (B) pure ethyl acetate. The gradient elution program was as follows: 0–16 min 0 %– 60 % A; 16–30 min 60 % A; 30–35 min 100 % A. The column temperature was kept at 25 °C, and the injection volume was 100 μL. Chromatograms were recorded in the range 300–700 nm and the EZ ChromeElite program was used for data processing. The identification of the pigments was done by comparison of their retention times and absorption spectra with reference spectra and commercial standards purchased from Sigma-Aldrich (Munich, Germany) or DHI Lab (Hørsholm, Denmark), which were also employed for the quantitative determination of the principal pigments found. Retinal-oxime standard was prepared from the bacteria *Salinibacter ruber* M13.When no

standards were available, the quantification of the pigments were done according to Zapata and coworkers [30]. All measurements were performed at least in triplicate and representative data is shown.

2.4. Genomic DNA Isolaton

For the isolation of genomic DNA, 2 L of each water sample were centrifuged at 19,800 ×*g* and the obtained pellet was used for the extraction of genomic DNA with the GeneJET Genomic Purification kit (Thermo Fisher Scientific, Waltham, MA, USA) following the manufacturer's instructions. The quantification of the genomic DNA and the assessment of its purity were done in a Nanodrop Spectrophotometer ND-1000 (Thermo Fisher Scientific). The four samples were then used for high throughput sequencing of 16S and 18S ribosomal RNA coding genes.

2.5. Libraries Preparation and DNA Sequencing

Prokaryotic and eukaryotic rDNA amplicons of specific hypervariable regions of the 16S rRNA and 18S rRNA coding genes were obtained by PCR amplification of the previously isolated genomic DNA with the Phusion® High-Fidelity PCR Master Mix (New England Biolabs, MA, USA). The hypervariable regions V3-V4 of the 16S rRNA and V9 of the 18S rRNA coding genes were amplified using the primer sets 341F/806R and 1380F/1510R, respectively (Table 1).

The primers used for the amplification of hypervariable regions of the 16S and 18S rDNA are shown, including the length of the amplified fragment and the primer sequences.

The quantity and quality of PCR products were analyzed by electrophoresis on 2 % agarose gel. PCR products were purified by the Qiagen Gel Extraction Kit (Qiagen, Germany) and pooled in equal ratios to generate two tagged libriries (one prokaryotic and one eukaryotic), with NEBNext® UltraTM DNA Library Prep Kit for Illumina and quantified via Qubit and Q-PCR. Finally, amplicons were sequenced on the Illumina MiSeq platform, using the Illumina MiSeq Reagent kit V2x 250 bp to generate paired-end raw reads. To keep the reliability of the data, quality controls were performed at each step of the procedure, from the raw DNA samples to the final data ($Q > 36$).

2.6. Sequence Data Processing

Bioinformatic data analysis was carried out using QIIME 2 (v2020.8) [31]. First of all, raw data were demultiplexed using the q2-demux plugin and filtered to get clean data, by trimming and truncating low-quality regions, dereplicating reads, and filtering chimeras, using DADA2 [32] (via q2-dada2). Then, the reads were organized in operational taxonomic units (OTUs) using de novo clustering method (via q2-vsearch) from VSEARCH [33]. The clustering was performed with a threshold identity value of 97 %, meaning that sequences that were 97 % identical to each other were grouped in the same OTUs. These OTUs were classified at each taxonomic rank using the q2-feature-classifier plugin (via the classify-sklearn method) and the SILVA database [34]. The SILVA (138.1) database was applied as two different pre-trained classifiers, specially curated, for 16S_V3-V4 and 18S_V9 regions. Annotation was performed with a 0.7 threshold. Venn diagrams representing common and specific taxons in the group of samples were obtained using the Venn Diagram package (v.1.6.20) for RStudio (v1.3.1093) and the data of the normalized OTUs. For the diversity analysis, the diversity alpha-rarefaction tool was used (via q2-diversity) to randomly select a different number of sequences and analyze the detected OTUs at each fraction to form a rarefaction curve. The core-metrics-phylogenetic tool (via q2-diversity) was also used to compute alpha diversity metrics. Biodiversity was estimated on the basis of the Shannon-Wiener diversity index (H).

Table 1
Description of regions and primers used for DNA sequencing.

Target	Region	Amplicon	Primer	Primer sequence (5′-3′)
18S rDNA	V9	131 pb	1380F	CCCTGCCHTTTGTACACAC
			1510R	CCTTCYGCAGGTTCACCTAC
16S rDNA	V3-V4	466 pb	341F	CCTAYGGGRBGCASCAG
			806R	GGACTACHVGGGTWTCTAAT

2.7. Statistical Analysis

Statistical studies were performed in IBM SPSS Statistics (v29). Correlation matrix and Principal Component Analysis (PCA) based on Bartlett's Test of Sphericity were used to study the relationships between the diverse data obtained along the salinity gradient.

3. Results

3.1. Sampling and Physicochemical Characterization of Water Samples

Four ponds of the Odiel Saltworks with increasing salt concentrations were sampled to perform this study. In coastal salterns, seawater is naturally evaporated over a series of connected ponds. In the first ponds, the less soluble salts, such as carbonates and sulfates, precipitate. Evaporation continues through the following pools until the point at which sodium chloride precipitates and can be harvested. Water samples were taken from: the seawater inlet (SWI), two different steps of the evaporation process (EP1 and EP2), and the crystallization pond (CP) (Fig. 1).

The main physicochemical parameters (conductivity, temperature, pH), as well as the total salinity, density, and brine composition of the collected samples, are shown in Table 2. Sodium chloride is clearly the main component of the brine, followed by magnesium chloride and magnesium sulfate, besides potassium chloride, calcium sulfate, and low levels of sodium bromide were also detected in the different sampled ponds. The salinity of the studied ponds is approximately 2-, 4- and 8-fold the salinity of the seawater, with total salt concentrations of 7.8, 14.4, and 31.8 %, respectively. As expected, density increases with salinity, rising from 1.025 g mL^{-1} in the seawater to 1.21 g mL^{-1} in the crystallization pond. Similarly, conductivity and the concentration of each individual salt increases with salinity, except the concentration of calcium sulfate, which is very insoluble and precipitates before reaching the crystallization pond. Temperature shows a slight increase, from 20 °C at the seawater inlet to 22 °C in the crystallization pond, which can be attributed to the slightly lower depth of this last pond, and pH shows little variation among the different sampled pools with a small decrease in the crystallization pond. As a result, salt-making works offer a set of ponds of increasing salinity, ranging from seawater, the most abundant environment on Earth, to saturated brine, one of the most extreme, in which most physicochemical parameters, except salinity, have very similar values, and given the shallow depth of the water in these ponds, there is no water stratification. Therefore, solar salterns constitute a particularly suitable system, for the simultaneous study of microbial biodiversity, pigment distribution, and relevance of photoheterotrophic metabolism throughout the whole salinity range.

Density, salinity, brine composition, conductivity, temperature, and pH are indicated for each sampling point. Values are the mean of three water samples (SD < 3 %). SWI, seawater inlet point; EP1 evaporation pond-1; EP2, evaporation pond-2; and CP, crystallization pond.

3.2. General Distribution of Pigments and Phytoplankton Across the Salinity Gradient

A general picture of pigments and phytoplankton distribution at different salinities was obtained from the absorption spectra of the acetone extracts and the fluorescence assisted flow cytometry analysis of the samples collected from the different ponds (Fig. 2). Both

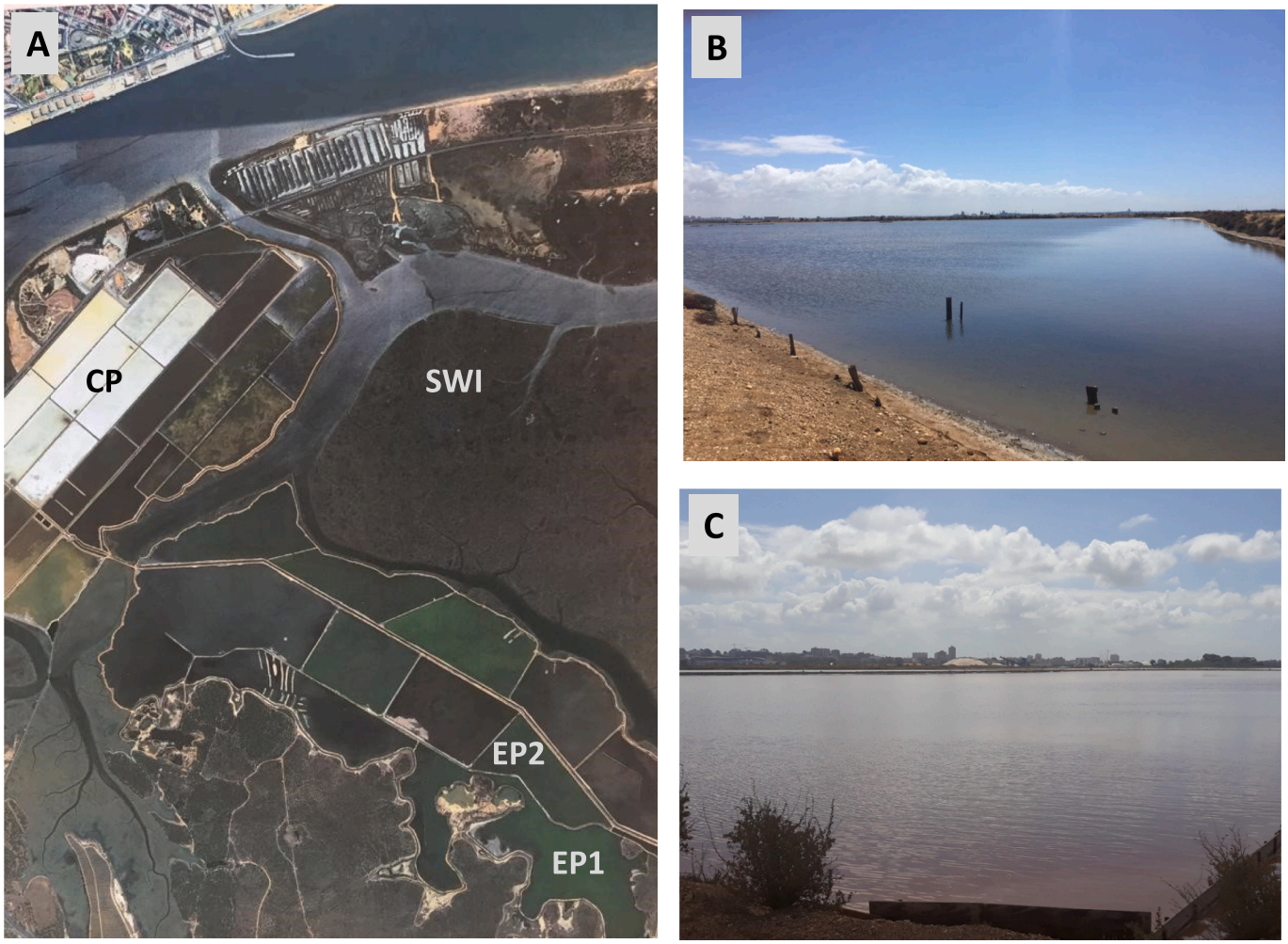

Fig. 1. Satellite view of Odiel Salterns and location of the sampling points at the seawater inlet point (SWI), two evaporation ponds (EP1, EP2), and the crystallization pond (CP) **(A)**. Images of two of the selected ponds: EP2 **(B)** and CP **(C)**, where the reddish color of the water at the highest salinity can be appreciated.

Table 2
Physicochemical parameters of the collected water samples.

Sample	Density (g•mL^{-1})	Salinity (%)	Brine Composition (g•L^{-1})						Cond. (mS•cm^{-1})	T^{a} (°C)	pH
			$CaSO_4$	$MgSO_4$	$MgCl_2$	NaCl	KCl	NaBr			
SWI	1.025	3.5	1.4	2.1	3.4	27.3	0.7	0.1	51	20	7.30
EP1	1.055	7.8	3.1	4.8	7.4	60.6	1.6	0.2	109	21	7.47
EP2	1.100	14.4	4.7	9.2	13.6	113.0	3.1	0.3	220	21	7.37
CP	1.210	31.8	1.6	21.1	30.8	256.8	7.0	0.8	241	22	6.99

phytoplankton and pigments profiles are strongly determined by the salinity.

The extracts from seawater (SWI) and the first evaporation pond (EP1) exhibit strong absorption in the range of 400–470 nm, with maxima at 450 nm and 670 nm. As salinity increases, in the EP2 and CP, the absorption spectrum experiments a shift to higher wavelengths. This is especially noticeable in the CP, at which the salt concentration reaches levels near saturation (~36 % *w/v*). At this salinity, the first maximum peak shifts from 450 to 500 nm, due to the presence of new carotenoids such as bacterioruberin. While the last peak, observed at 670, which is characteristic of chlorophylls, practically disappears. In the crystallization pond, the absorption spectrum of the acetone extract is practically like that of bacterioruberin, denoting the total dominance of this pigment, the main carotenoid of haloarchaea (Fig. 2).

Besides, profiling of phytoplankton single cells analyzed by fluorescence assisted flow cytometry allowed the discrimination of different photosynthetic populations according to their size and pigment content. Chlorophyll detection was based on the red autofluorescence (FL3, 670 nm), while phycoerythrins, characteristics of cyanobacteria, red algae, and cryptophytes were recognized by their orange fluorescence (FL2, 585 nm). The highest number of photosynthetic cells ($1.4•10^6$ cells•mL^{-1}) was registered at 7.8 % salinity, decreasing at higher salinities. Photosynthetic cells encountered in the crystallization pond ($4.4•10^4$ cells•mL^{-1}) were much lower than the cells found in the seawater ($6.9•10^5$ cells•mL^{-1}). Phycoerythrin-containing cells were particularly abundant at an intermediate salinity in the EP1 (Fig. 2). This result is in agreement with the information obtained from metabarcoding, which revealed that the phylum cyanobacteria supposes 21 % of the prokaryotic population of the EP1, as discussed below. The cellular density of phytoplankton was particularly low in the CP, coinciding with the disappearance of the maximum at 670 in the absorption spectrum, which corresponds to chlorophylls.

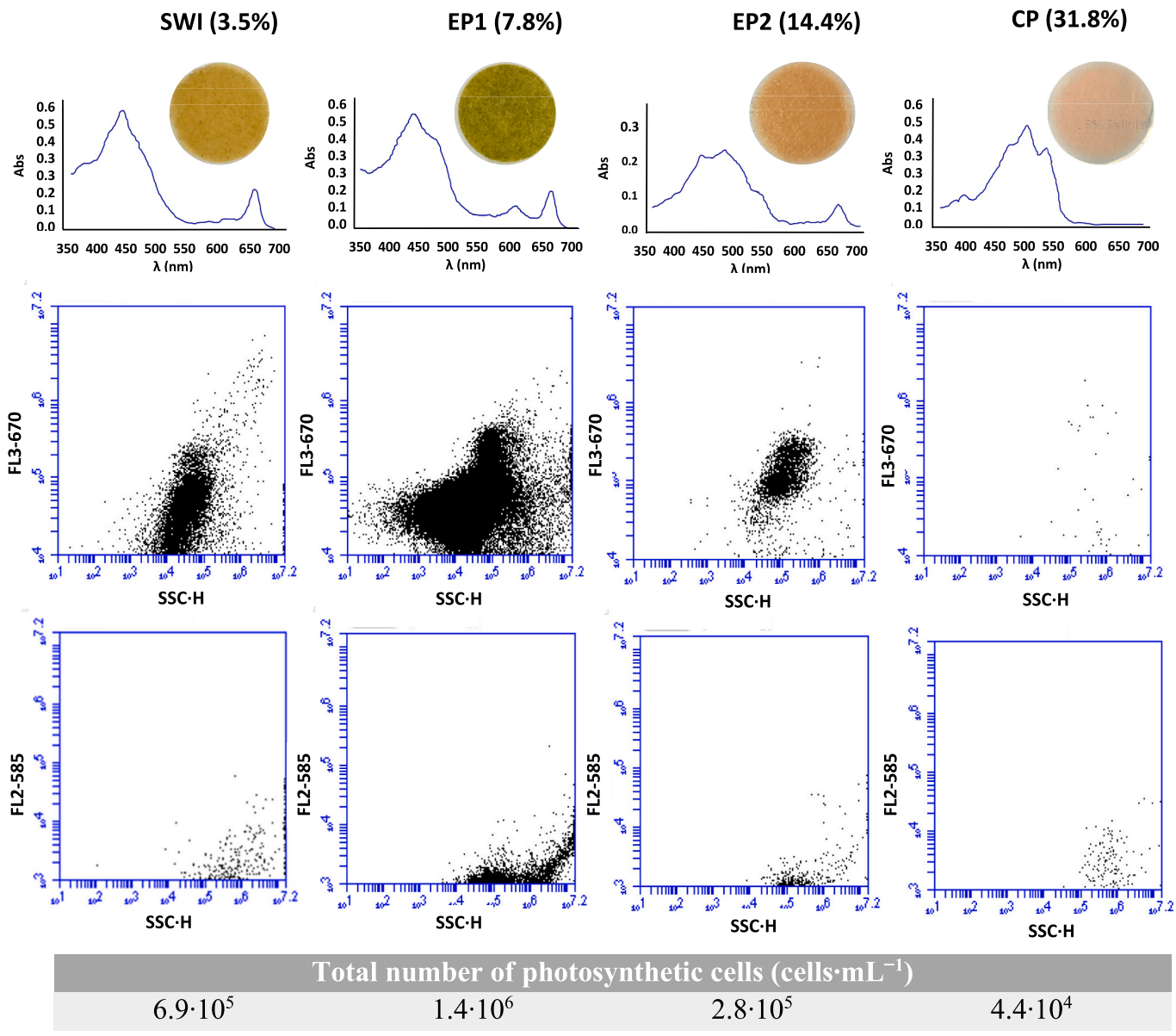

Fig. 2. UV–Vis spectra of the acetonic extracts (top) and density plots representing red fluorescence (FL3, 670 nm) vs. side scatter (SSC) (center) and orange fluorescence (FL2, 585 nm) vs. side scatter (SSC) (down) for the saltern ponds analyzed; SWI: 3.5 % salinty; EP1: 7.8 % salinty; EP2: 14.4 % salinity, and CP: 31.8 % salinty). The coloration of glass microfiber filters used for biomass collection at each salinity and the total concentration of photosynthetic cells encountered in each sample are also shown. (For interpretation of the references to color in this figure legend, the reader is referred to the web version of this article)

3.3. Variations in the Pigment Composition in Response to Salinity Levels

To get further insight into the influence of salinity in the pigment profile, the main components of the extracts obtained at each salinity were identified by RP-HPLC (Fig. 3, Supplementary Material Table S1) and feature pigments were quantified (Supplementary Material Table S2). The results showed that chlorophyll *a* and *b* were present at all the studied salinities, with their maxima in the EP1, at 7.8 % salinity. Similarly, lutein and zeaxanthin were the main carotenoids found in the EP1, and considerably abundant in the SWI and in the EP2. Bacterioruberin appeared at 14.4 % salinity in the EP2 and was the main carotenoid recorded in the CP, at 31.8 % salinity, while salinixanthin was only detected at the highest salinity. In addition, several xanthophylls, such as fucoxanthin, neoxanthin, violaxanthin, diadinoxanthin, and diatoxanthin, representative of different phytoplankton groups, were identified in the SWI and the EP1. Chlorophyll *c* and the ketocarotenoid siphonaxanthin were only observed in the SWI sample, while canthaxanthin was exclusively present at 7.8 % salinity (EP1). Finally, β-carotene was found in small quantities in all the samples, with its maximum in the CP (Fig. 3, Supplementary Material Table S2).

The presence of these signature pigments is a good taxonomic marker to identify the composition of the microbial community at each salinity. In this sense, fucoxanthin indicated the presence of diatoms, and similarly, chlorophyll *c*, diadinoxanthin, and diatoxanthin revealed the presence of dinoflagellates and diatoms. Likewise, zeaxanthin noted the inhabitance of cyanobacteria, bacterioruberin highlighted the existence of haloarchaea, and salinixanthin pointed out the inhabitance of the halophilic bacteria *Salinibacter*. Chlorophyll *b* and lutein marked the prevalence of green microalgae, while chlorophyll *a* is considered an indicator of whole oxygenic photosynthetic microbiota [35,36]. Other carotenoids detected, like violaxanthin, neoxanthin, and β-carotene, are usually present in diverse photosynthetic microorganisms, including chlorophytes, prasinophytes, and some dinoflagellates, whereas siphonaxanthin is a dominant pigment in prasinophytes [37].

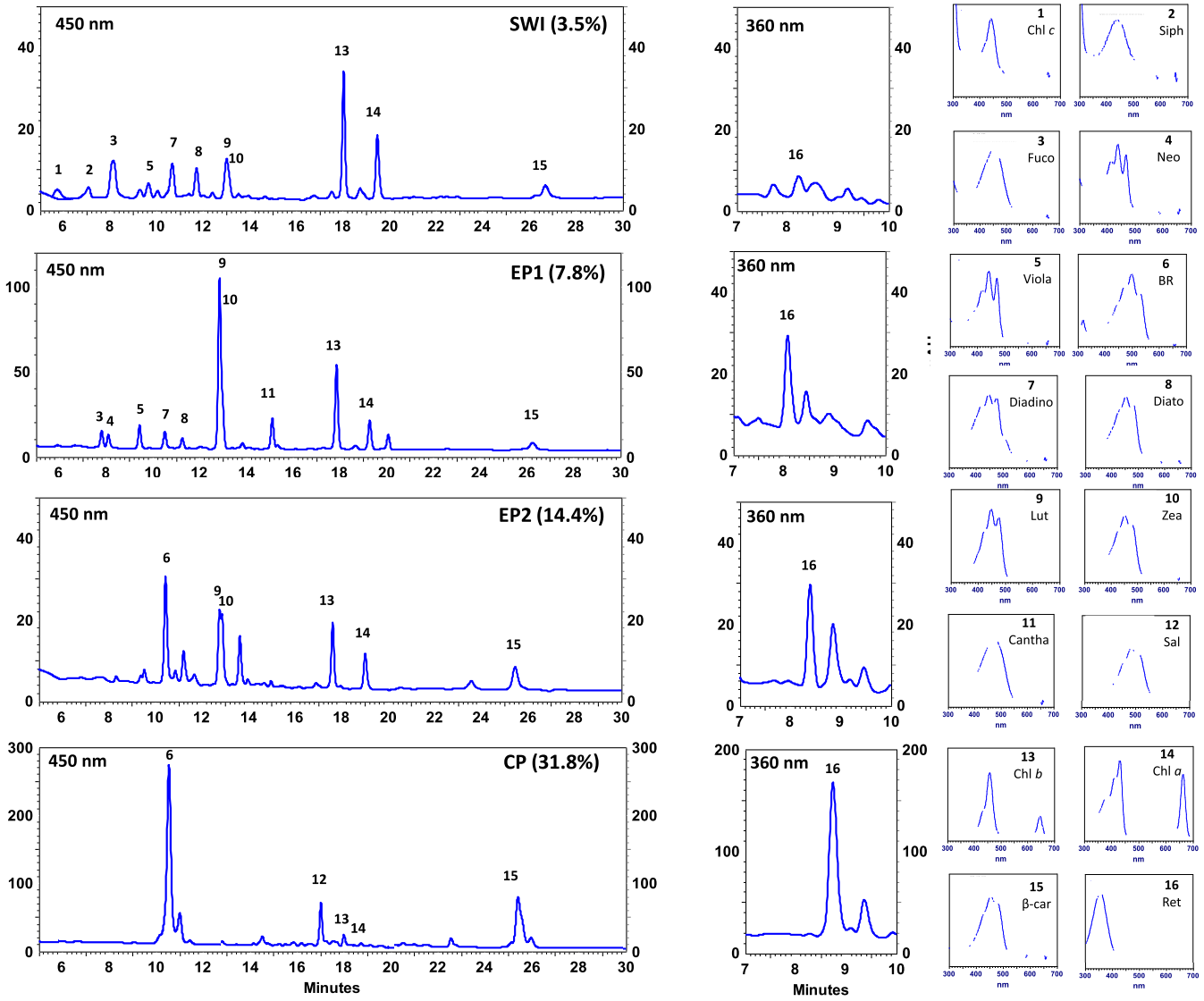

Fig. 3. HPLC elution profiles of the pigments at 450 nm (left panel) and retinal-oxime at 360 nm (central panel) obtained from the biomass recovered at the indicated salinities SWI: 3.5 % salinty; EP1: 7.8 % salinty; EP2: 14.4 % salinity, and CP: 31.8 % salinity.The UV–vis spectra of the main pigments are also shown (right panel), including chlorophyll *c* (1), siphonaxanthin (2), fucoxanthin (3), neoxanthin (4), violaxanthin (5), bacterioruberin (6), diadinoxanthin (7), diatoxanthin (8), lutein (9), zeaxanthin (10), canthaxanthin (11), salinixanthin (12), chlorophyll *b* (13), chlorophyll *a* (14), β-carotene (15), retinal-oxime (16).

3.4. Analysis of Relative Chlorophyll a / Retinal Abundance

In addition to chlorophyll *a* and signature pigments, the concentration of retinal in the samples from the four salinities was studied (Fig. 3-central panel). In this case, chloroform/methanol extracts were treated with hydroxylamine to obtain retinal-oxyme, which was determined by HPLC as indicated in 2.3. As salinity increased, the retinal content exhibits an important rise, being especially noticeable at very high salinity (Fig. 3, Supplementary Material Table S2). The relative significance of the two main mechanisms for solar energy photoconversion in the sea, chlorophyll *a*-based oxygenic photosynthesis (Fig. 4A) and retinal-based rhodopsin systems (Fig. 4B), can be estimated from the determination of the concentrations of retinal and chlorophyll *a*. Therefore, molar retinal/chlorophyll *a* ratio was calculated at different salinities (Fig. 4, Table S2). Following the assumptions made by Gómez-Consarnau and coworkers [11], which take into account that all known rhodopsins have a single retinal chromophore associated with the rhodopsin while in each photosynthetic unit there are around 300 molecules for Chl *a* per reaction center, and also previous estimations that suggest that about 80 % of the quantified retinal is bound to proton pumping rhodopsins, being the other 20 % linked to sensory rhodopsins, the effective retinal/Chl *a* ratio, understood as the light energy harvesting capability of each transduction system, can be estimated as follows:

$$\text{Effective Retinal : Chl a Ratio} = \frac{[\text{Retinal}] \times 300}{[\text{Chl a}] \times 1.25}$$

The molar concentration of retinal and chlorophyll *a*, as well as the molar effective ratio at each salinity, are shown in Fig. 4. It can be observed that the concentration of Chl *a* is higher than that of retinal in all the studied salinities except for the highest one, 31.8 %, at which the concentration of retinal is 20 times higher. Nonetheless, the effective ratio retinal:Chl *a*, is always considerably much higher than one, indicating the relevance of the retinal-based energy transducing mechanism over the Chl-*a*-based photosynthesis. Furthermore, this effective ratio increases exponentially with the salinity, reaching in the CP 2200 times the value observed in the SWI.

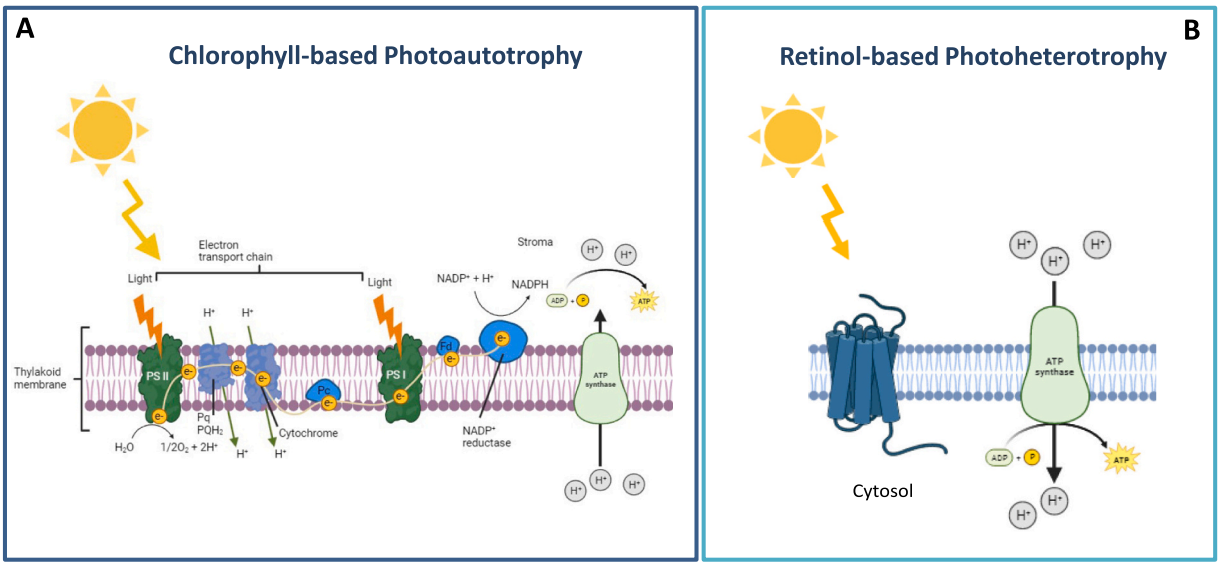

C

Salinity	3.5%	7.8%	14.4%	31.8%
Retinal (nmol·L^{-1})	0.11	18.90	7.71	46.05
Chlorophyll *a* (nmol·L^{-1})	11.66	39.45	9.56	2.14
Molar Ratio Ret:Chl *a*	0.01	0.48	0.81	21.52
Effective Ratio Ret:Chl *a*	2.33	115.03	193.45	5165.06

Fig. 4. Scheme of the chlorophyll-based (A) and retinal-based (B) mechanisms for capture of solar energy at different salinities. Ratios and concentration of retinal (as retinal oxime) and chlorophyll *a* at each sampled ponds (C). Values are the mean of three determinations (SD < 5 %). Effective retinal/chlorophyll *a* ratio is calculated by the expression: ([Retinal] × 300)/([Chl *a*] × 1.25).

3.5. High Throughput Sequencing of rDNA Marker Genes

To complete the study, the microbial diversity of the three domains of life, *Bacteria*, *Archaea*, and *Eukarya*, proliferating at the four studied ponds, was characterized by next-generation sequencing of the 16S rRNA and 18S rRNA marker genes, as detailed in Materials and Methods. Sequencing of the generated libraries gave rise to a series of paired-end raw reads with mean lengths of 416 bp for prokaryotes (16S rRNA gene) and 269 pb for eukaryotes (18S rRNA gene). The bioinformatics processing of the sequences for assembling, denoising, filtering, and elimination of chimeras and artifacts, performed as detailed in Material and Methods, generated the effective tags, which were finally grouped by 97 % DNA sequence similarity into operational taxonomic units (OTUs). The number of input reads, effective tags, and final OTUs for each sample are shown in Fig. 5A. Finally, the OTUs were annotated and the identified taxons with their relative abundance are shown in Supplementary Material Table S3.

As shown in Fig. 5A, the number of OTUs observed in both, eukaryotes and prokaryotes, comes down as salinity increases, with an exception for eukaryotes in the CP that experienced a rise with respect to the EP2. The number of prokaryotic taxons was higher than the number of eukaryotic ones in all the sampled ponds. This superiority was particularly noticeable in the samples from the EPs. Fig. 5A also shows the Shannon diversity index (H) for the prokaryotic and eukaryotic populations at each studied salinity, while the rarefaction curves are shown in Supplementary Material Fig. S1. The Shannon diversity index combines richness and diversity, measuring the number of taxonomic groups and the disparity between them. High Shannon index values indicate the presence of many species with well-balanced abundances [38]. As shown in Fig. 5A, the highest biodiversity values were found in seawater, where Shannon values were slightly higher for eukaryotes (6.30) than for prokaryotes (5.50). However, it should be noted that eukaryotic diversity declined sharply in the EP1 and EP2 and showed a slight increase at the highest salinity (CP). Contrarily, the diversity of prokaryotes presented a sustained decline as salinity increased, showing higher Shannon values than eukaryotes along the whole salinity gradient, indicating a higher diversity of prokaryotic species at all the studied salinities.

Furthermore, the common and the unique taxa in the different salinities were plotted in Venn diagrams for prokaryotes (Fig. 5B) and eukaryotes (Fig. 5C). Seawater (SWI) was the sample that showed more unique taxons, which were not found at higher salinities, for both groups of microorganisms. Concerning prokaryotic microorganisms, the samples that shared more taxons were those from the evaporation ponds with intermedium salinities (7.8 and 14.4 %) (Fig. 5B). While for eukaryotes, the samples with more common taxons were those with the nearest salinities, 3.5 with 7.8 %, and 14.4 with 31.8 % (Fig. 5C).

3.6. Prokaryotic Community Composition

16S metataxonomic high-throughput analysis was performed to identify the prokaryotic microorganisms through the salinity gradient (Fig. 6). At the lowest salinities, 3.5 and 7.8 %, *Bacteria* accounted for almost 99 % of the prokaryotic population, while their abundance decreased to 77 % and 42 % in the EP1 and the CP, respectively. Instead, *Archaea* was the dominant group in the CP, representing 58 % of the total prokaryotes (Fig. 6A). The analysis of the main phyla in the prokaryotic domain revealed that the phylum *Proteobacteria* was dominant at all salinities, except at the highest one, where it was not even present. At seawater, the phylum *Proteobacteria* represented 90 % of the prokaryotic population, but its abundance decreased to around 35–40 % in the EP1 and EP2 (Fig. 6B). At saturating salt conditions (CP), only two main phyla could be distinguished, *Bacteroidetes* and *Euryarcheaota*, which is one of the main archaeal phyla.

A deeper analysis of the most abundant prokaryotic OTUs in the dominant phylum at each salinity allowed their classification into family

A

Pond	Salinity	Sample	Input tags	Effective tags	OTUs	Shannon index
SWI	3.5%	16S rDNA	206,161	171,476	647	5.50
		18S rDNA	203,677	109,547	556	6.30
EP-1	7.8%	16S rDNA	180,896	137,118	573	5.00
		18S rDNA	202,348	81,710	71	1.25
EP-2	14.4%	16S rDNA	198,989	115,081	406	4.45
		18S rDNA	201,047	164,568	69	1.40
CP	31.8%	16S rDNA	180,896	12,635	170	3.85
		18S rDNA	200,352	149,139	133	2.90

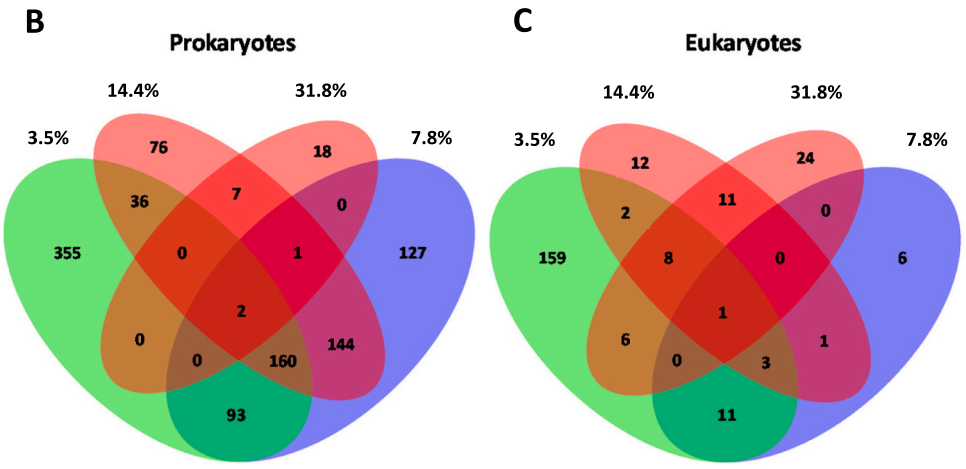

Fig. 5. Sequencing statistics. The number of inputs, non-chimeric de-noised merged inputs (effective tags) Observed Operational Taxonomic Units (OTUs), and Shannon indexes (H) obtained are shown for each sample, including the four salinities and the two groups, prokaryotes (16S rRNA) and eukaryotes (18S rRNA) (A). Venn diagrams with the number of identified taxons for prokaryotes and eukaryotes at each of the studied salinities (3.5, 7.8, 14.4, and 31.8 %) are also shown for prokaryotes (B) and eukaryotes (C). Values in the overlapping zones in the Venn diagrams represent normalized common taxons, while the others are specific taxons in each sample. All samples exhibited Q > 30.

and genus (Fig. 6C). At seawater salinity, twelve different genera classified in eight families with relative abundance higher than 1 % were identified. The major bacteria found at this salinity belong to the genus *Stenotrophomonas* and to an uncultured member of the family *Pelagibacteraceae*, which together formed almost half of the entire proteobacteria population. In the EP1 (7.8 % salinity), the majority of the proteobacteria community belonged to the family *Rhodobacteraceae*. Nonetheless, when salinity reached 14.4 % (EP2), the genus *Spiribacter*, which was a minority in the EP1, became predominant. Finally, in the CP, the prokaryotic population was composed of a great variety of haloarchaea (~60 %), with *Halorubrum*, *Haloquadratum*, and *Halonotius* as the dominant genera, and only two representatives of bacteria, among which *Salinibacter* (39 %) was clearly predominant (Fig. 6C).

3.7. Eukaryotic Community Composition

The metabarcoding study of the 18S rRNA coding gene revealed that the phylum *Chlorophyta* was absolutely dominant among the eukaryotes at all the studied salinities, exceeding 95 % in the evaporation ponds (EP1, EP2) (Fig. 7A). Other remarkable members of phytoplankton found in the seawater sample were diatoms, included in the phylum *Ochrophyta*, as well as, dinoflagellates, such as the genus *Alexandrinum* (8 %), and protalveolates, like *Parvilucifera* (7 %), belonging to the phylum *Miozoa*. Non-photosynthetic eukaryotes were only perceptible at low salinity. In seawater, fungi species of the phyla *Basidiomycota* and *Ascomycota* represented around 2 %, while the phylum *Amoebozoa* accounted for 1 % of total eukaryotes. All these genera and their relative percentages are detailed in Supplementary Material Table S3.

Further taxonomic analysis of the phylum *Chlorophyta* through the salinity gradient showed that the main representatives belonged to the classes *Chlorophyceae* and *Trebouxiophyceae*. *Picochlorum* was the predominant genus in the SWI, EP1, and EP2, with a relative abundance of 57, 99, and 78 %, respectively. By contrast, *Dunaliella* was the main genus found at the highest salinity (CP), with 83 % of relative abundance. The presence of this microalgae has been extensively reported in environments with saturating salt concentration, where it is considered the primary producer [39,40]. In seawater, other microalgae found in a minor proportion belonged to marine species of the genera *Tetraselmis* and *Chlamydomonas*. The appearance of the genus *Blidingia,* a multicellular alga of the family *Kornmanniaceae*, in this study could be due to the presence of rests or spores from this seaweed in the seawater sample. In addition to the identified microalgae, it should be noted that in the SWI uncharacterized chlorophytes were found in considerable abundance (Fig. 7B).

3.8. Statistical and Comparative Analyses

The combined analysis of the different obtained data allows stablishing correlations among the abundance of prokaryotes and eukaryotes, the chlorophyll *a*/retinal ratio and the salinity (Table 3), and between the most abundant phyla and pigments at each salinity (Fig. 8). The heat map correlation matrix offers a global view of the microbial

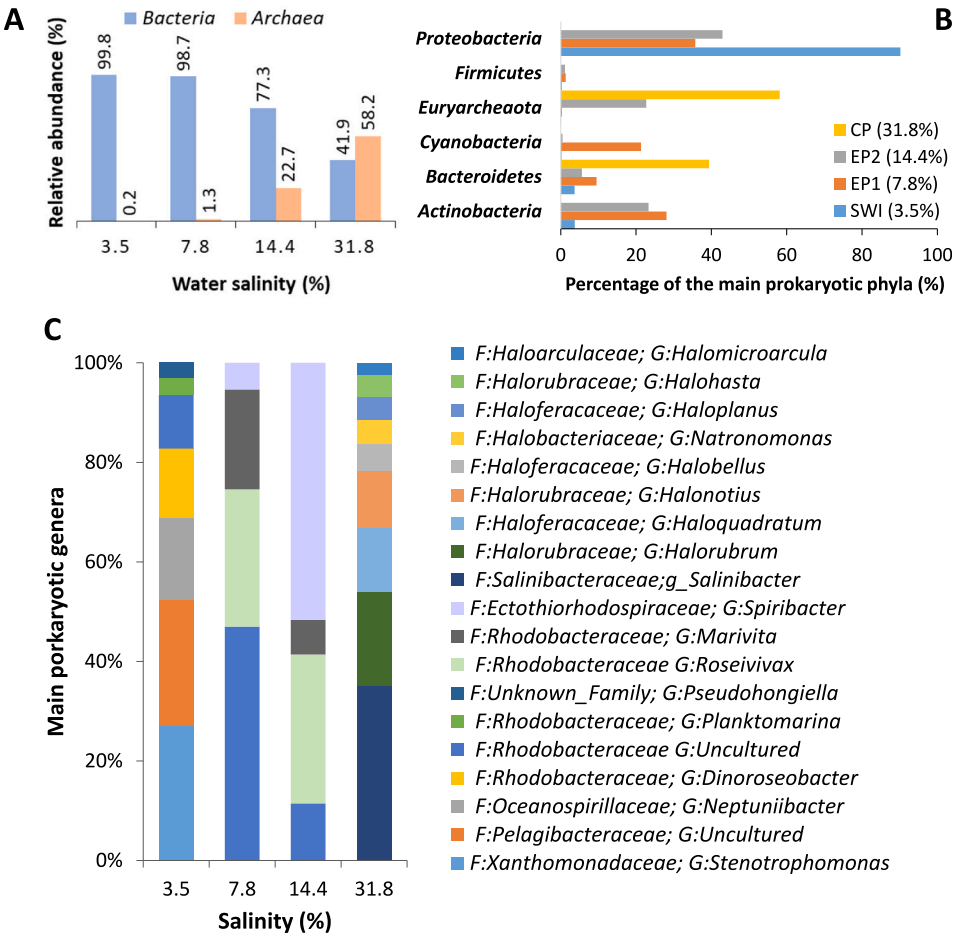

Fig. 6. Distribution of the prokaryotic representatives across the salinity gradient (salinities of 3.5, 7.8, 14.4, and 31.8 %). Relative abundance of the *Bacteria* and *Archaea* domains (A). The main phyla (with more than 1 % of relative abundance) represented alphabetically (B). Relative abundance of the main genera found in the dominant prokaryotic phylum at each salinity (C), indicating their taxonomic classification, family (F), and genus (G).

profiles and the contribution of different solar light transduction mechanisms across the salinity gradient in the Odiel solar salterns (Table 3). The negative correlation between salinity, the number of OTUs, and the Shannon biodiversity indexes for both prokaryotes and eukaryotes, indicates the decrease in species-richness as salinity increases. Similarly, the content of chlorophyll *a* and phytoplankton correlate negatively with salinity, denoting a reduction in the energy captured by photosynthesis when salinity rises. On the contrary, the retinal content and the calculated effective retinal/Chl *a* ratio have a strong positive correlation with salinity, which points to the expansion of photoheterotrophy in sunlight capturing as salinity increases.

In addition, the PCA of the main phyla and pigments at each salinity, shown in Fig. 8, confirms that there is a strong correlation between detected signature pigments and the abundance of the corresponding microorganisms identified in the metabarcoding study, and makes evident that three main groups can be distinguished with accordance to the salinity, divided into low (3.4 %), medium (7.8 % and 14.4 %), and high (31.8 %) salinity (Fig. 8).

4. Discussion

Extreme hypersaline ecosystems harbor a wide variety of halophilic microorganisms that can be a potential source of valuable molecules, such as poly-extremophilic enzymes and carotenoids, useful for many biotechnological applications [25,26,41,42]. A better understanding of the microbiology of saltern ponds may reveal details about the mechanisms they use to tolerate high concentrations of salt and to capture solar energy in these challenging conditions. To our knowledge, this work entails the first insights into the prokaryotic and eukaryotic microbial dynamics through the salinity gradient in coastal Atlantic solar salterns and a pioneer study of the relevance of photoheterotrophy in hypersaline habitats.

The retinal/chlorophyll ratios observed at different salinities in this study confirm that microbial rhodopsin-based photoheterotrophy is the main contributor to the solar energy capture on the surface of the sea, as has been already reported in the Mediterranean Sea [11], and show that its importance is progressively higher as salinity increases, reaching a maximum at the CP, in which the salinity is near saturation (Fig. 4). The remarkable decrease in the concentration of photosynthetic microorganisms at the EP2 and the CP observed by flow cytometry (Fig. 2) joined to the bloom of haloarchaea and *Salinibacter*, microorganisms that possess light-driven proton pumps, are strong indicators that photoheterotrophy is the overriding mechanism in this extreme environment. The negative correlation of salinity with photosynthesis and species-richness as salinity increases is highlighted in the correlation matrix (Table 3), as expected for extreme environments [43]. Instead, retinal-based photoheterotrophy has a strong positive correlation with salinity, which remarks the boost of photoheterotrophy as salinity increases. Moreover, the high effective retinal/Chl *a* ratio at the CP, which becomes 2200 times the value observed in seawater offers an idea of the quantitative importance of this mechanism for capturing sunlight energy, which could get even more importance in areas where the salinity is raising due to climate change. Previous studies suggest the high significance of rhodopsin-based phototrophy under starvation of nutrients,

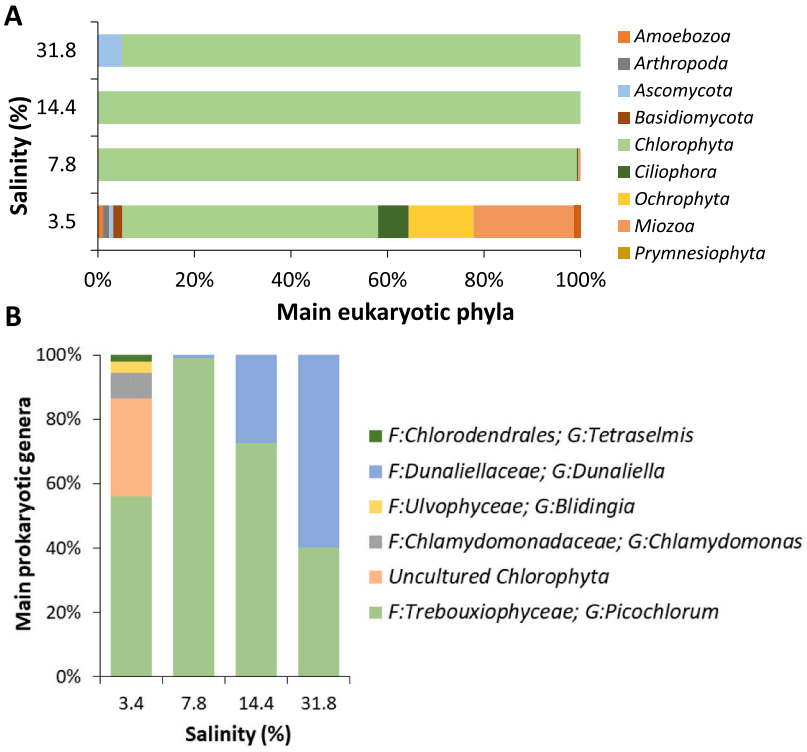

Fig. 7. Distribution of the eukaryotic community across the salinity gradient salinities of 3.5, 7.8, 14.4, and 31.8 %. Percentage of the main phyla (with more than 1 % of relative abundance) for each salinity alphabetically presented (A). Relative abundance of the main genera of the phylum *Chlorophyta* through the salinity gradient, family (F), and genus (G) of the members found (B).

Table 3
Heat map correlation matrix among the normalized values of the main parameters studied through the salinity.

	Salinity	Total OTUs	OTUs Prokarya	OTUs Eukarya	H Index Prokarya	H Index Eukarya	Phyto-plankton	Chl *a*	Retinal	Eff. Ratio Ret:Chl*a*
Salinity	**1.00**	-0.83	-0.99	-0.48	-0.96	-0.55	-0.38	-0.57	0.98	0.99
Total OTUs	-0.83	**1.00**	0.86	0.89	0.94	0.35	-0.06	0.18	-0.70	-0.76
OTUs Prokarya	-0.99	0.86	**1.00**	0.53	0.98	0.62	0.40	0.60	-0.94	-0.98
OTUs Eukarya	-0.48	0.89	0.53	**1.00**	0.67	0.02	-0.46	-0.24	-0.31	-0.38
H Index Prokarya	-0.96	0.94	0.98	0.67	**1.00**	0.57	0.27	0.49	-0.88	-0.94
H Index Eukarya	-0.55	0.35	0.62	0.02	0.57	**1.00**	0.85	0.92	-0.48	-0.64
Phytoplankton	-0.38	-0.06	0.40	-0.46	0.27	0.85	**1.00**	0.97	-0.43	-0.51
Chlorophyll *a*	-0.57	0.18	0.60	-0.24	0.49	0.92	0.97	**1.00**	-0.59	-0.69
Retinal	0.98	-0.70	-0.94	-0.31	-0.88	-0.48	-0.43	-0.59	**1.00**	0.97
Eff. Ratio Ret:Chl*a*	0.99	-0.76	-0.98	-0.38	-0.94	-0.64	-0.51	-0.69	0.97	**1.00**

Heat map correlation matrix with the obtained data including the number of OTUs (total, prokaryotic, and eukaryotic), the biodiversity Shannon index (H) for prokarya and eukarya, the content of retinal and Chl a, and the calculated effective ratio retinal:Chl a. Possitive values are indicated in green, while negative values are shown in reddish colors.

such as carbon [44] or iron [45]. However, the extraordinary increase of the retinal/Chl *a* ratio observed at high salinity has never been reported.

The strong correlation of signature pigments with the microorganisms identified in the metabarcoding study shown in the PCA (Fig. 8), allows the establishment of three groups based on their distribution according to salinity, including low (3.4 %), medium (7.8 % and 14.4 %), and high (31.8 %) salinity. For example, diatoms and dinoflagellates that belong to the phyla *Ochrophyta* and *Miozoa*, respectively, which are the second and third most abundant phyla in seawater (Fig. 7A), grouped with pigments only detected at this salinity, such as chlorophyll *c*, and with the features pigments fucoxanthin, diadinoxanthin, and diatoxanthin, observed in the SWI and the EP1, but much more abundant in seawater (Fig. 3).

Similarly, cyanobacteria are one of the main prokaryotic phyla detected in the EP1 (Fig. 6B), in agreement with the high content of canthaxanthin and zeaxanthin at medium salinity within the second PCA group (Fig. 3, Fig. 8), also reinforced by the presence of phycoerythrins observed in the flow cytometry assay at this salinity (Fig. 2). These results are in consonance with the surveys carried out in Santa Pola salterns (Spain), where the phytoplankton presented the most abundant population at 8 % salinity [46] and other salterns ponds with moderate salinities [47]. Moreover, lutein and chlorophyll *b*, correlate well with the dominance of *Chlorophyta* among the eukaryotic community especially in the EP1 and EP2 (Fig. 7A), with the great

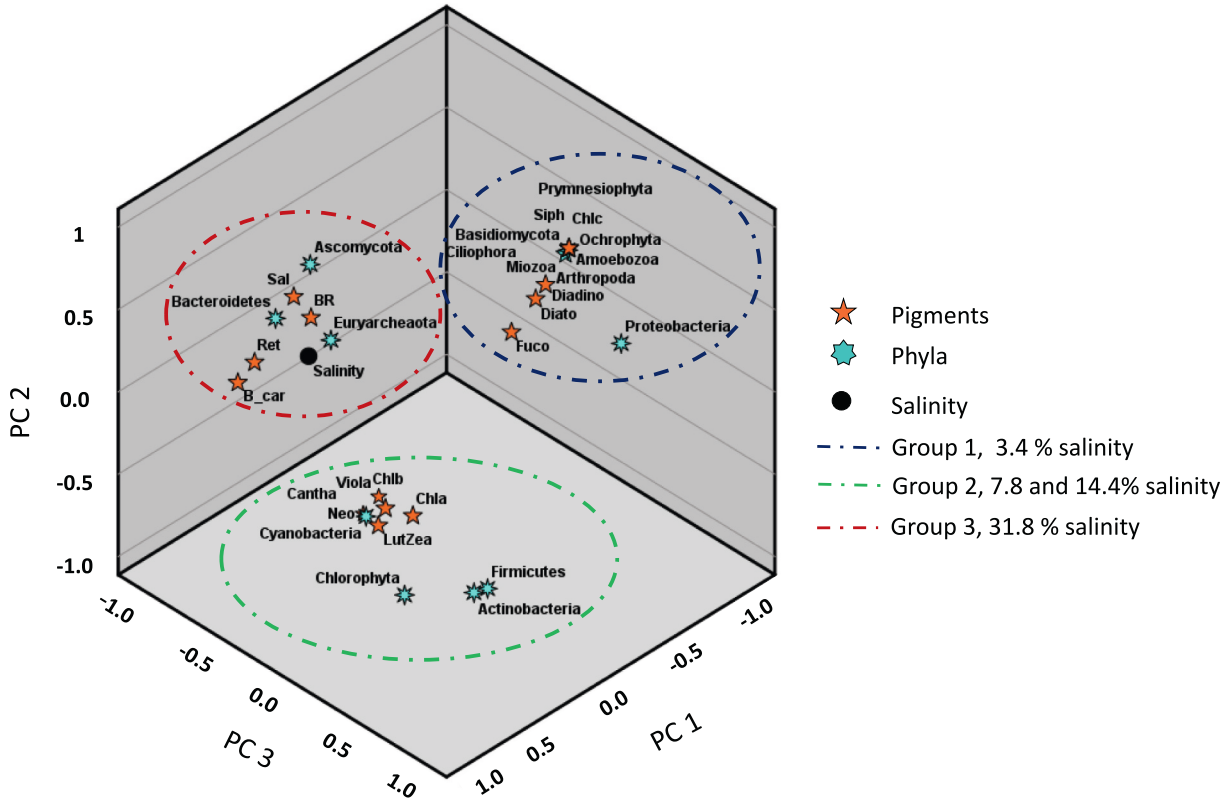

Fig. 8. Principal component analysis showing the relationships between the quantified pigments and phyla with salinity. Three main groups are remarked according to the scores obtained.

dominance of the green microalga *Picochlorum* (Fig. 7B). Microalgae of this genus are halotolerant and usually grow in brackish water from marshlands and other hypersaline habitats with salinity fluctuations [48,49].

Finally, in the third group of the PCA, it is shown the strong correlation of salinity with the pigments retinal, bacterioruberin, and salinixanthin, found in the CP and the phyla *Euryarcheaota* and *Bacteroidetes*, which includes haloarchaea and the halophilic bacteria *Salinibacter*, respectively. In addition, although β-carotene is present in all the salinity, its maximum was recorded in the CP, where species of the halophilic microalgae *Dunaliella* proliferate (Fig. 7). Previous findings from crystallizer ponds in different locations, shown in Table 4, have demonstrated that bacterioruberin is usually the major carotenoid at saturating salinity [50]. In this case, it is necessary to take into account that, unlike bacterioruberin, salinixanthin usually appears tightly bound in an equimolar ratio to the retinal protein xanthorhodopsin, acting as an accessory chromophore [51] and consequently, salinixanthin content per cell is usually low [52].

The great wealth of haloarchaea in hypersaline habitats has been widely reported [18,53], whereas, the population of *Salinibacter* varies

Table 4
Percentage of the main prokaryotic **(A)** and eukaryotic **(B)** phyla reported in different locations through an increasing salinity gradient.

Mean salinity	4 %			8 %			14 %			28 %		
Prokaryota	SP·AT	IN	POL	SP·AT	IN	POL	SP·AT	IN	POL	SP·AT	IN	POL
Actinobacteria	4	1	0	28	1	0	2	0	0	0	0	0
Bacteroidetes	4	13	10	10	0	13	6	9	28	34	8	28
Cyanobacteria	0	0	0	0	0	21	1	6	0	0	0	0
Euryarcheota	0	34	0	1	0	15	23	51	49	58	90	90
Firmicutes	1	6	0	0	0	1	1	18	0	0	0	0
Proteobacteria	90	36	90	36	0	72	43	10	21	0	1	22

Mean salinity	4 %			8 %			14 %			28 %		
Eukaryota	SP·AT	AU	SP·MD	SP·AT	AU	SP·MD	SP·AT	AU	SP·MD	SP·AT	AU	SP·MD
Alveolata	21	18	32	0	15	0	0	90	0	0	0	0
Chlorophyta	41	12	10	98	5	0	95	10	0	66	95	95
Fungi	2	5	38	0	0	0	0	0	0	5	0	0
Ochrophyta	10	56	10	0	75	0	0	0	0	3	0	0
Prymnesiophyta	1	15	5	0	0	0	0	0	0	0	0	0

Distribution of the main prokaryotic and eukaryotic phyla through an increasing salinity gradient in: Atlantic Odiel salterns in Spain (**SP·AT**, present study), Goa salterns in India (**IN**) [58], Ciechocinek spa in Poland (**POL**) [56], salty lakes [23,59] in Australia (**AU**), Mediterranean Sea [60], and Santa Pola salterns [46] in Spain (**SP·MED**).

substantially between the different locations. Similarly to our findings, the abundance of *Salinibacter* in the Saltern of Margherita di Savoia (Italy) was around 40 % at very high salinities [54]. By contrast, in other hypersaline habitats the maximum concentration of this species was up to 17 % [55], and not even detected in Poland [56]. Diverse reports support that green algae (*Chlorophyte*) and alveolates (*Miozoa*) conform usually the eukaryotic community of hypersaline systems, always being *Dunaliella* the predominant at the highest salinity [23,46,57]. Geographic conditions, brine composition, and specific microbial interactions could be responsible for the observed differences, as shown in the comparative analysis of the few reports that describe the dynamics of the dominant microbial phyla across the salinity gradient at different locations around the world, including in solar salterns in India [58], brine graduation tanks in Poland [56], Santa Pola salterns in the Mediterranean coast of Spain [46], and salty lakes of Australia [23,59], summarized in Table 4.

5. Conclusions

This research entails an exhaustive study of microbial populations over a wide range of salinities, from seawater to hypersaline water near saturation, an extreme environment where only specially adapted microorganisms can proliferate and that constitute a valuable source of unique compounds and biological processes for multiple biotechnological purposes. The composition of microbial communities at each salinity was obtained by a combination of metataxonomy, cytometry, and pigment analyses that showed well-correlated data. Our results demonstrate that, in general, microbial pigments are good indicators to reveal the main inhabitants at each salinity, allowing the comparison between pigmented populations such as microalgae, cyanobacteria, and extreme halophilic archaea and bacteria, which are the main representatives at intermedium and high salinities. Finally, our pioneer study of the evolution of sunlight harvesting systems along the salinity gradient disclosed the progressively outstanding role of retinal-based photoheterotrophy over photosynthesis as salinity increases. Although the amount of the harvested solar energy transformed into specific biological functions has not been addressed in this study, we showed that the uptake of radiant energy to the biosphere by retinal-based photoheterotrophy in this extreme ecosystem is undoubtedly of utmost importance, especially when photosynthetic microorganisms are scarce at the highest salinities. Further challenges will be the determination of how proteorhodopsin photoheterotrophy influences global energy and carbon cycling, especially in sunlit oligotrophic locations, where this mechanism is exceptionally valuable.

Funding

This research was funded by MICIU/AEI/ 10.13039/501100011033, ERDF/EU (research grant PID2022-140995OB-C21), and Research Project for Young Sea Researchers (CEIMAR-2022).

CRediT authorship contribution statement

Patricia Gómez-Villegas: Writing – review & editing, Writing – original draft, Methodology, Investigation, Conceptualization. **Miguel Pérez-Rodríguez:** Investigation. **Jesús M. Porres:** Writing – review & editing, Funding acquisition. **José C. Prados:** Writing – review & editing, Funding acquisition. **Consolación Melguizo:** Writing – review & editing, Supervision, Funding acquisition. **Javier Vigara:** Writing – review & editing, Supervision, Funding acquisition. **Ignacio Moreno-Garrido:** Writing – review & editing, Investigation. **Rosa León:** Writing – review & editing, Writing – original draft, Supervision, Funding acquisition, Conceptualization.

Declaration of competing interest

The authors declare that they have no known competing financial interests or personal relationships that could have appeared to influence the work reported in this paper.

Data availability

Metadata are submitted to Dryad. Gómez Villegas, Patricia et al. (Forthcoming 2024). Dryad. https://doi.org/10.5061/dryad.m63xsj431

Acknowledgments

The authors thank to “Salinas del Odiel S.L.” company and E. Martinez-Montes and L. Refojo of the “Paraje Natural Marismas del Odiel” for their support in obtaining the water samples used in this study; Josefa Antón and Cristina López from the University of Alicante for providing *Salinibacter* M13 cells for the isolation of salinixanthin standard; and R. Fernández for graphic design. P. Gómez-Villegas acknowledges the financial support of the University of Huelva for the “Margarita Salas Grant”. Funding for open access charge: Universidad de Huelva / CBUA is acknowledged.

Appendix A. Supplementary data

Supplementary data to this article can be found online at https://doi.org/10.1016/j.jphotobiol.2024.113043.

References

[1] O.M. Finkel, O. Béjà, S. Belkin, Global abundance of microbial rhodopsins, ISME J. 7 (2013) 448–451, https://doi.org/10.1038/ismej.2012.112.
[2] D. Oesterhelt, W. Stoeckenius, Rhodopsin-like protein from the purple membrane of *Halobacterium halobium*, Nat. New Biol. 233 (1971) 149–152, https://doi.org/10.1038/newbio233149a0.
[3] O. Béjà, L. Aravind, E.V. Koonin, M.T. Suzuki, A. Hadd, L.P. Nguyen, S. B. Jovanovich, C.M. Gates, R.A. Feldman, J.L. Spudich, E.N. Spudich, E.F. DeLong, Bacterial rhodopsin: evidence for a new type of phototrophy in the sea, Science 289 (2000) 1902–1906, https://doi.org/10.1126/science.289.5486.1902.
[4] O. Béjà, E.N. Spudich, J.L. Spudich, M. Leclerc, E.F. DeLong, Proteorhodopsin phototrophy in the ocean, Nature 411 (2001) 786–789, https://doi.org/10.1038/35081051.
[5] S.P. Balashov, E.S. Imasheva, V.A. Boichenko, J. Antón, J.M. Wang, J.K. Lanyi, Xanthorhodopsin: a proton pump with a light-harvesting carotenoid antenna, Science 309 (2005) 2061–2064, https://doi.org/10.1126/science.1118046.
[6] A. Rozenberg, K. Inoue, H. Kandori, O. Béjà, Microbial Rhodopsins: the last two decades, Ann. Rev. Microbiol. 75 (2021) 427–447, https://doi.org/10.1146/annurev-micro-031721-020452.
[7] T. Balandin, D. Volkov, A. Alekseev, K. Kovalev, D. Bratanov, V. Gordeliy, *E. coli* Expression and Purification of Microbial and Viral Rhodopsins, 2022, https://doi.org/10.1007/978-1-0716-2329-9_5.
[8] B. Brindefalk, M. Ekman, K. Ininbergs, C.L. Dupont, S. Yooseph, J. Pinhassi, B. Bergman, Distribution and expression of microbial rhodopsins in the Baltic Sea and adjacent waters, Environ. Microbiol. 18 (2016) 4442–4455, https://doi.org/10.1111/1462-2920.13407.
[9] A. Vader, H.D. Laughinghouse, C. Griffiths, K.S. Jakobsen, T.M. Gabrielsen, Proton-pumping rhodopsins are abundantly expressed by microbial eukaryotes in a high-Arctic fjord, Environ. Microbiol. 20 (2018) 890–902, https://doi.org/10.1111/1462-2920.14035.
[10] M. Ma, H. Li, C. Wang, T. Li, J. Wang, H. Yuan, L. Yu, J. Wang, L. Li, S. Lin, A comparative study reveals the relative importance of prokaryotic and eukaryotic proton pump rhodopsins in a subtropical marginal sea, ISME Commun. 3 (2023) 1–9, https://doi.org/10.1038/s43705-023-00292-y.
[11] L. Gómez-Consarnau, J.A. Raven, N.M. Levine, L.S. Cutter, D. Wang, B. Seegers, J. Arístegui, J.A. Fuhrman, J.M. Gasol, S.A. Sañudo-Wilhelmy, Microbial rhodopsins are major contributors to the solar energy captured in the sea, Sci. Adv. 5 (2019) 1–8, https://doi.org/10.1126/sciadv.aaw8855.
[12] A. Chazan, I. Das, T. Fujiwara, S. Murakoshi, A. Rozenberg, A. Molina-Márquez, F. K. Sano, T. Tanaka, P. Gómez-Villegas, S. Larom, A. Pushkarev, P. Malakar, M. Hasegawa, Y. Tsukamoto, T. Ishizuka, M. Konno, T. Nagata, Y. Mizuno, K. Katayama, R. Abe-Yoshizumi, S. Ruhman, K. Inoue, H. Kandori, R. León, W. Shihoya, S. Yoshizawa, M. Sheves, O. Nureki, O. Béjà, Phototrophy by antenna-containing rhodopsin pumps in aquatic environments, Nature (2023), https://doi.org/10.1038/s41586-023-05774-6.
[13] M. Tamm, R. Freiberg, I. Tõnno, P. Nõges, T. Nõges, Pigment-based chemotaxonomy - a quick alternative to determine algal assemblages in large

shallow eutrophic lake? PLoS One 10 (2015) 1–15, https://doi.org/10.1371/journal.pone.0122526.
[14] A. Oren, Halophilic microbial communities and their environments, Curr. Opin. Biotechnol. 33 (2015) 119–124, https://doi.org/10.1016/j.copbio.2015.02.005.
[15] S. Boutaiba, H. Hacene, K.A. Bidle, J.A. Maupin-Furlow, Microbial diversity of the hypersaline Sidi Ameur and Himalatt Salt Lakes of the Algerian Sahara, J. Arid Environ. 75 (2011) 909–916, https://doi.org/10.1016/j.jaridenv.2011.04.010.
[16] M. Hugoni, A. Escalas, C. Bernard, S. Nicolas, D. Jézéquel, F. Vazzoler, G. Sarazin, C. Leboulanger, M. Bouvy, P. Got, M. Ader, M. Troussellier, H. Agogué, Spatiotemporal variations in microbial diversity across the three domains of life in a tropical thalassohaline lake (Dziani Dzaha, Mayotte Island), Mol. Ecol. 27 (2018) 4775–4786, https://doi.org/10.1111/mec.14901.
[17] R. Ghai, C.M. Hernandez, A. Picazo, C.M. Mizuno, K. Ininbergs, B. Díez, R. Valas, C. L. Dupont, K.D. McMahon, A. Camacho, F. Rodriguez-Valera, Metagenomes of mediterranean coastal lagoons, Sci. Rep. 2 (2012), https://doi.org/10.1038/srep00490.
[18] H. Baati, S. Guermazi, R. Amdouni, N. Gharsallah, A. Sghir, E. Ammar, Prokaryotic diversity of a Tunisian multipond solar saltern, Extremophiles 12 (2008) 505–518, https://doi.org/10.1007/s00792-008-0154-x.
[19] S. Çınar, M.B. Mutlu, Comparative analysis of prokaryotic diversity in solar salterns in eastern Anatolia (Turkey), Extremophiles 20 (2016) 589–601, https://doi.org/10.1007/s00792-016-0845-7.
[20] J.H. Jacob, E.I. Hussein, M.A.K. Shakhatreh, C.T. Cornelison, Microbial community analysis of the hypersaline water of the Dead Sea using high-throughput amplicon sequencing, Microbiologyopen 6 (2017) e00500, https://doi.org/10.1002/mbo3.500.
[21] L. Butinar, S. Sonjak, P. Zalar, A. Plemenitaš, N. Gunde-Cimerman, Melanized halophilic fungi are eukaryotic members of microbial communities in hypersaline waters of solar salterns, Bot. Mar. 48 (2005) 73–79, https://doi.org/10.1515/BOT.2005.007.
[22] E. Alexander, A. Stock, H.W. Breiner, A. Behnke, J. Bunge, M.M. Yakimov, T. Stoeck, Microbial eukaryotes in the hypersaline anoxic L'Atalante deep-sea basin, Environ. Microbiol. 11 (2009) 360–381, https://doi.org/10.1111/j.1462-2920.2008.01777.x.
[23] K.B. Heidelberg, W.C. Nelson, J.B. Holm, N. Eisenkolb, K. Andrade, J.B. Emerson, Characterization of eukaryotic microbial diversity in hypersaline lake tyrrell, Australia, Front. Microbiol. 4 (2013) 115, https://doi.org/10.3389/fmicb.2013.00115.
[24] F. Zhao, S. Filker, Characterization of protistan plankton diversity in ancient salt evaporation ponds located in a volcanic crater on the island Sal, Cape Verde, Extremophiles 22 (2018) 943–954, https://doi.org/10.1007/s00792-018-1050-7.
[25] P. Gómez-Villegas, J. Vigara, L. Romero, C. Gotor, S. Raposo, B. Gonçalves, R. Léon, Biochemical characterization of the amylase activity from the new haloarchaeal strain haloarcula sp. HS isolated in the odiel marshlands, Biology (Basel) 10 (2021) 337, https://doi.org/10.3390/biology10040337.
[26] P. Gómez-Villegas, J. Vigara, M. Vila, J. Varela, L. Barreira, R. Léon, Antioxidant, antimicrobial, and bioactive potential of two new Haloarchaeal strains isolated from Odiel Salterns (Southwest Spain), Biology (Basel). 9 (2020) 298, https://doi.org/10.3390/biology9090298.
[27] B. Vera-Gargallo, A. Ventosa, Metagenomic insights into the phylogenetic and metabolic diversity of the prokaryotic community dwelling in hypersaline soils from the Odiel saltmarshes (SW Spain), Genes (Basel) 9 (2018) 152, https://doi.org/10.3390/genes9030152.
[28] P. Gómez-Villegas, J. Vigara, R. León, Characterization of the microbial population inhabiting a solar Saltern pond of the Odiel marshlands (SW Spain), Mar. Drugs 16 (2018) 332, https://doi.org/10.3390/md16090332.
[29] W.S.M. El-Sayed, S. Takaichi, H. Saida, M. Kamekura, M. Abu-Shady, H. Seki, T. Kuwabara, Effects of light and low oxygen tension on pigment biosynthesis in *Halobacterium salinarum*, revealed by a novel method to quantify both retinal and carotenoids, Plant Cell Physiol. 43 (2002) 379–383, https://doi.org/10.1093/pcp/pcf044.
[30] M. Zapata, F. Rodríguez, J.L. Garrido, Separation of chlorophylls and carotenoids from marine phytoplankton: a new HPLC method using a reversed phase C8 column and pyridine-containing mobile phases, Mar. Ecol. Prog. Ser. 195 (2000) 29–45, https://doi.org/10.3354/meps195029.
[31] E. Bolyen, J.R. Rideout, M.R. Dillon, N.A. Bokulich, C.C. Abnet, G.A. Al-Ghalith, H. Alexander, E.J. Alm, M. Arumugam, F. Asnicar, Y. Bai, J.E. Bisanz, K. Bittinger, A. Brejnrod, C.J. Brislawn, C.T. Brown, B.J. Callahan, A.M. Caraballo-Rodríguez, J. Chase, E.K. Cope, R. Da Silva, C. Diener, P.C. Dorrestein, G.M. Douglas, D. M. Durall, C. Duvallet, C.F. Edwardson, M. Ernst, M. Estaki, J. Fouquier, J. M. Gauglitz, S.M. Gibbons, D.L. Gibson, A. Gonzalez, K. Gorlick, J. Guo, B. Hillmann, S. Holmes, H. Holste, C. Huttenhower, G.A. Huttley, S. Janssen, A. K. Jarmusch, L. Jiang, B.D. Kaehler, K. Bin Kang, C.R. Keefe, P. Keim, S.T. Kelley, D. Knights, I. Koester, T. Kosciolek, J. Kreps, M.G.I. Langille, J. Lee, R. Ley, Y.-X. Liu, E. Loftfield, C. Lozupone, M. Maher, C. Marotz, B.D. Martin, D. McDonald, L.J. McIver, A.V. Melnik, J.L. Metcalf, S.C. Morgan, J.T. Morton, A.T. Naimey, J. A. Navas-Molina, L.F. Nothias, S.B. Orchanian, T. Pearson, S.L. Peoples, D. Petras, M.L. Preuss, E. Pruesse, L.B. Rasmussen, A. Rivers, M.S. Robeson, P. Rosenthal, N. Segata, M. Shaffer, A. Shiffer, R. Sinha, S.J. Song, J.R. Spear, A.D. Swafford, L. R. Thompson, P.J. Torres, P. Trinh, A. Tripathi, P.J. Turnbaugh, S. Ul-Hasan, J.J. J. van der Hooft, F. Vargas, Y. Vázquez-Baeza, E. Vogtmann, M. von Hippel, W. Walters, Y. Wan, M. Wang, J. Warren, K.C. Weber, C.H.D. Williamson, A. D. Willis, Z.Z. Xu, J.R. Zaneveld, Y. Zhang, Q. Zhu, R. Knight, J.G. Caporaso, Reproducible, interactive, scalable and extensible microbiome data science using QIIME 2, Nat. Biotechnol. 37 (2019) 852–857, https://doi.org/10.1038/s41587-019-0209-9.
[32] B.J. Callahan, P.J. McMurdie, M.J. Rosen, A.W. Han, A.J.A. Johnson, S.P. Holmes, DADA2: high-resolution sample inference from Illumina amplicon data, Nat. Methods 13 (2016) 581–583, https://doi.org/10.1038/nmeth.3869.
[33] T. Rognes, T. Flouri, B. Nichols, C. Quince, F. Mahé, VSEARCH: a versatile open source tool for metagenomics, PeerJ 2016 (2016) 1–22, https://doi.org/10.7717/peerj.2584.
[34] C. Quast, E. Pruesse, P. Yilmaz, J. Gerken, T. Schweer, P. Yarza, J. Peplies, F. O. Glöckner, The SILVA ribosomal RNA gene database project: improved data processing and web-based tools, Nucleic Acids Res. 41 (2013) D590–D596, https://doi.org/10.1093/nar/gks1219.
[35] C. Chai, T. Jiang, J. Cen, W. Ge, S. Lu, Phytoplankton pigments and functional community structure in relation to environmental factors in the Pearl River estuary, Oceanologia 58 (2016) 201–211, https://doi.org/10.1016/j.oceano.2016.03.001.
[36] A. Damar, F. Colijn, K.J. Hesse, F. Kurniawan, Coastal phytoplankton pigments composition in three tropical estuaries of Indonesia, J. Mar. Sci. Eng. 8 (2020), https://doi.org/10.3390/JMSE8050311.
[37] G. Britton, S. Liaaen-Jensen, H. Pfander, Carotenoids, 1st ed., Birkhäuser Basel, Basel, 2004 https://doi.org/10.1007/978-3-0348-7836-4.
[38] A.D. Willis, Rarefaction, alpha diversity, and statistics, Front. Microbiol. 10 (2019) 2407, https://doi.org/10.3389/fmicb.2019.02407.
[39] R. Elevi Bardavid, P. Khristo, A. Oren, Interrelationships between Dunaliella and halophilic prokaryotes in saltern crystallizer ponds, Extremophiles 12 (2008) 5–14, https://doi.org/10.1007/s00792-006-0053-y.
[40] S. Keerthi, U.D. Koduru, S.S. Nittala, N.R. Parine, The heterotrophic eubacterial and archaeal co-inhabitants of the halophilic *Dunaliella salina* in solar salterns fed by bay of Bengal along south eastern coast of India, Saudi, Aust. J. Biol. Sci. 25 (2018) 1411–1419, https://doi.org/10.1016/j.sjbs.2015.10.019.
[41] A. Oren, Industrial and environmental applications of halophilic microorganisms, Environ. Technol. 31 (2010) 825–834, https://doi.org/10.1080/09593330903370026.
[42] P.P. Kanekar, S.P. Kanekar, A.S. Kelkar, P.K. Dhakephalkar, Halophiles – taxonomy, diversity, physiology and applications, in: Microorg. Environ. Manag., Springer, Netherlands, Dordrecht, 2012, pp. 1–34, https://doi.org/10.1007/978-94-007-2229-3_1.
[43] S. Frontier, Diversity and structure in aquatic ecosystems, Oceanogr. Mar. Biol. Annu. Rev. 23 (1985) 253–312.
[44] R. Bar-Shalom, A. Rozenberg, M. Lahyani, B. Hassanzadeh, G. Sahoo, M. Haber, I. Burgsdorf, X. Tang, V. Squatrito, L. Gomez-Consarnau, O. Béjà, L. Steindler, Rhodopsin-mediated nutrient uptake by cultivated photoheterotrophic Verrucomicrobiota, ISME J. 17 (2023) 1063–1073, https://doi.org/10.1038/s41396-023-01412-1.
[45] J. Strauss, L. Deng, S. Gao, A. Toseland, C. Bachy, C. Zhang, A. Kirkham, A. Hopes, R. Utting, E.F. Joest, A. Tagliabue, C. Löw, A.Z. Worden, G. Nagel, T. Mock, Plastid-localized xanthorhodopsin increases diatom biomass and ecosystem productivity in iron-limited surface oceans, Nat. Microbiol. 8 (2023) 2050–2066, https://doi.org/10.1038/s41564-023-01498-5.
[46] M. Estrada, P. Henriksen, J.M. Gasol, E.O. Casamayor, C. Pedrós-Alió, Diversity of planktonic photoautotrophic microorganisms along a salinity gradient as depicted by microscopy, flow cytometry, pigment analysis and DNA-based methods, FEMS Microbiol. Ecol. 49 (2004) 281–293, https://doi.org/10.1016/j.femsec.2004.04.002.
[47] K.B. Sørensen, D.E. Canfield, A.P. Teske, A. Oren, Community composition of a hypersaline endoevaporitic microbial mat, Appl. Environ. Microbiol. 71 (2005) 7352–7365, https://doi.org/10.1128/AEM.71.11.7352-7365.2005.
[48] M. de la Vega, E. Díaz, M. Vila, R. León, Isolation of a new strain of Picochlorum sp and characterization of its potential biotechnological applications, Biotechnol. Prog. 27 (2011) 1535–1543, https://doi.org/10.1002/btpr.686.
[49] J. Nana Annan, Growth and photosynthesis response of the green alga, Picochlorum oklahomensis to iron limitation and salinity stress, Int. J. Plant Physiol. Biochem. 6 (2014) 7–18, https://doi.org/10.5897/IJPPB2013.0198.
[50] A. Oren, F.F. Rodríguez-Valera, The contribution of halophilic Bacteria to the red coloration of saltern crystallizer ponds1, FEMS Microbiol. Ecol. 36 (2001) 123–130, https://doi.org/10.1111/j.1574-6941.2001.tb00832.x.
[51] J.K. Lanyi, S.P. Balashov, Xanthorhodopsin: a bacteriorhodopsin-like proton pump with a carotenoid antenna, Biochim. Biophys. Acta Bioenerg. 1777 (2008) 684–688, https://doi.org/10.1016/j.bbabio.2008.05.005.
[52] A. Oren, The microbiology of red brines, in: Adv. Appl. Microbiol., 1st ed., Elsevier Inc., 2020, pp. 57–110, https://doi.org/10.1016/bs.aambs.2020.07.003.
[53] J. Zhang, G. Ma, Y. Deng, J. Dong, G. Van Stappen, L. Sui, Bacterial diversity in Bohai Bay solar Saltworks, China, Curr. Microbiol. 72 (2016) 55–63, https://doi.org/10.1007/s00284-015-0916-5.
[54] C. Leoni, M. Volpicella, B. Fosso, C. Manzari, E. Piancone, M.C.G. Dileo, E. Arcadi, M. Yakimov, G. Pesole, L.R. Ceci, A differential metabarcoding approach to describe taxonomy profiles of bacteria and archaea in the saltern of Margherita di savoia (Italy), Microorganisms 8 (2020) 1–20, https://doi.org/10.3390/microorganisms8060936.
[55] M.R. del Mora-Ruiz, A. Cifuentes, F. Font-Verdera, C. Pérez-Fernández, M.E. Farias, B. González, A. Orfila, R. Rosselló-Móra, Biogeographical patterns of bacterial and archaeal communities from distant hypersaline environments, Syst. Appl. Microbiol. 41 (2018) 139–150, https://doi.org/10.1016/j.syapm.2017.10.006.
[56] A. Kalwasińska, E. Deja-Sikora, A. Burkowska-But, A. Szabó, T. Felföldi, P. Kosobucki, A. Krawiec, M. Walczak, Changes in bacterial and archaeal communities during the concentration of brine at the graduation towers in Ciechocinek spa (Poland), Extremophiles 22 (2018) 233–246, https://doi.org/10.1007/s00792-017-0992-5.

[57] E.O. Casamayor, X. Triadó-Margarit, C. Castañeda, Microbial biodiversity in saline shallow lakes of the Monegros Desert, Spain, FEMS Microbiol. Ecol. 85 (2013) 503–518, https://doi.org/10.1111/1574-6941.12139.

[58] K. Mani, N. Taib, M. Hugoni, G. Bronner, J.M. Bragança, D. Debroas, Transient dynamics of archaea and bacteria in sediments and brine across a salinity gradient in a solar saltern of Goa, India, Front. Microbiol. 11 (2020) 1–19, https://doi.org/10.3389/fmicb.2020.01891.

[59] S. Balzano, E. Abs, S.C. Leterme, Protist diversity along a salinity gradient in a coastal lagoon, Aquat. Microb. Ecol. 74 (2015) 263–277, https://doi.org/10.3354/ame01740.

[60] H. Liu, N. Risgaard-Petersen, U. Sommer, M. Moustaka-Gouni, N. Stefanidou, S. Genitsaris, J. Lopez-Bautista, Unicellular eukaryotic community response to temperature and salinity variation in Mesocosm experiments, Front. Microbiol. 9 (2018) 2444, https://doi.org/10.3389/fmicb.2018.02444.